How to cite: *Angew. Chem. Int. Ed.* **2022,** *61,* e202205801
International Edition: doi.org/10.1002/anie.202205801
German Edition: doi.org/10.1002/ange.202205801

Molecular Motors

The Influence of Strain on the Rotation of an Artificial Molecular Motor

Michael Kathan, Stefano Crespi, Axel Troncossi, Charlotte N. Stindt, Ryojun Toyoda, and Ben L. Feringa**

Abstract: In artificial small-molecule machines, molecular motors can be used to perform work on coupled systems by applying a mechanical load—such as strain—that allows for energy transduction. Here, we report how ring strain influences the rotation of a rotary molecular motor. Bridging the two halves of the motor with alkyl tethers of varying sizes yields macrocycles that constrain the motor's movement. Increasing the ring size by two methylene increments increases the mobility of the motor stepwise and allows for fine-tuning of strain in the system. Small macrocycles (8–14 methylene units) only undergo a photochemical *E*/*Z* isomerization. Larger macrocycles (16–22 methylene units) can perform a full rotational cycle, but thermal helix inversion is strongly dependent on the ring size. This study provides systematic and quantitative insight into the behavior of molecular motors under a mechanical load, paving the way for the development of complex coupled nanomachinery.

[*] Dr. M. Kathan, Dr. S. Crespi, A. Troncossi, C. N. Stindt, Dr. R. Toyoda, Prof. Dr. B. L. Feringa
Stratingh Institute for Chemistry, University of Groningen
Nijenborgh 4, 9747 AG Groningen (The Netherlands)
E-mail: b.l.feringa@rug.nl

Dr. M. Kathan
Present address: Department of Chemistry, Humboldt-Universität zu Berlin
Brook-Taylor-Str. 2, 12489 Berlin (Germany)
E-mail: michael.peter.kathan@chemie.hu-berlin.de

Dr. S. Crespi
Present address: Department of Chemistry—Ångström Laboratory, Uppsala University
Box 523, 751 20 Uppsala (Sweden)

Dr. R. Toyoda
Present address: Department of Chemistry, Graduate School of Science, Tohoku University
6-3 Aramaki-Aza-Aoba, Aobaku, Sendai 980-8578 (Japan)

Introduction

Biological molecular machines (BMMs)[1,2] perform a variety of vital tasks in living organisms, such as driving the formation of energy carriers (ATP synthase), transporting cellular cargo (kinesin) or synthesizing proteins (ribosome). Taking BMMs as an example, a key challenge for artificial molecular machines (AMMs)[3–9] is to perform work on a coupled system, i.e. transducing the energy that is put into the system into other forms of energy, by avoiding heat dissipation as efficiently as possible.[5,8,10,11] In recent years, molecular machinists developed AMMs that can execute more and more sophisticated tasks, such as multifunctional catalysis,[12–14] contracting or moving macroscopic objects,[15–22] penetrating and affecting cell walls,[23–25] transporting and assembling molecular entities,[26–29] shifting chemical equilibria,[30,31] performing coupled motions[32–37] or pumping molecular entities.[38–43]

As demonstrated in the examples above, photochemical molecular motors[44–50] can be crucial components in AMMs. They are utilized as energy converters able to transduce light into other forms of energy.[11] The working mechanism of Feringa-type molecular motors is based on light-induced configurational isomerization of a chiral overcrowded alkene, which can adopt two different helicities in both of its stereoisomers (*E* and *Z*, Figure 1A). Upon light illumination, the *Z* stable (s) molecule undergoes an *E*/*Z* isomerization to form an *E* metastable (m) isomer with inverted helicity, which then relaxes in a thermal step by helix inversion (THI) to the *E*s isomer. This process corresponds to a directed 180° rotation. To close a full 360° rotational cycle the molecule needs to undergo a second *E*/*Z* isomerization (this time from the *E*s to *Z*m isomer) followed by a subsequent THI from the *Z*m to *Z*s diastereomer. Constant exposure to light leads to continuous unidirectional rotary motion, the direction of which is governed by a chiral sp^3-hybridized carbon center in the allylic position of the molecule.

In the case of our molecular motors, the challenge is to couple them to an external load, so that their light-driven unidirectional motion can be harnessed to perform work on a coupled system.[8] One possible way to achieve this target is by constraining the motion of the motor, i.e. applying a mechanical load, so that parts of the motor movement are converted into, for instance, coupled motion[33–37,51] or chemical strain[17,31,52–59] of a secondary molecular entity. Detailed mechanistic studies of photochemical molecular motors that perform work against a mechanical load, applied

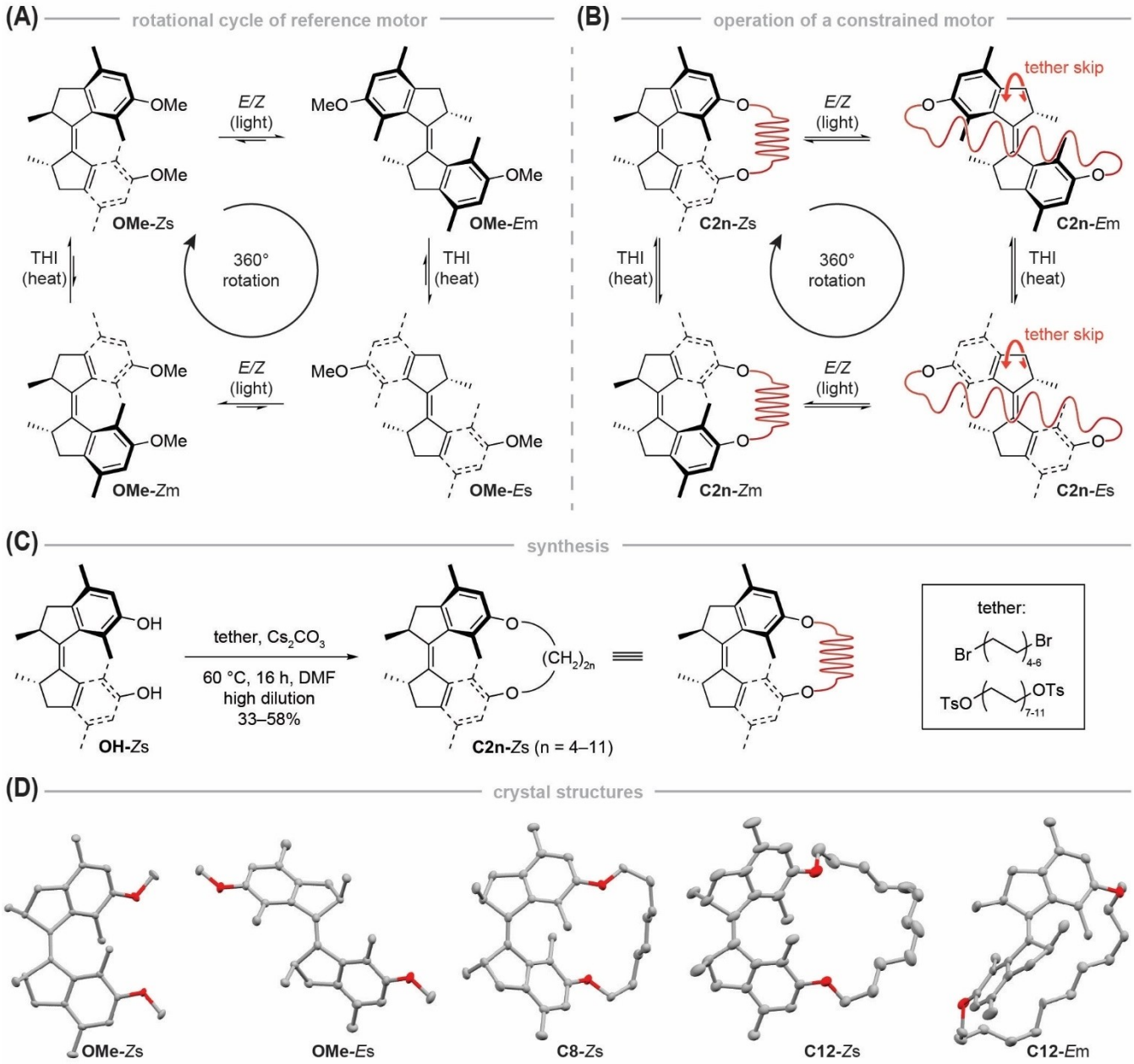

Figure 1. Operational routine, synthesis and structural characterization of motor macrocycles. A) Full rotational cycle of unconstrained motor **OMe**. Starting from the *Z*s isomer, the motor undergoes an *E*/*Z* isomerization upon UV light illumination, followed by a subsequent THI that converts **OMe**-*Em* into **OMe**-*Es*. Subsequent UV light illumination forms the *Z*m isomer, which undergoes another THI to form the starting isomer *Z*s. B) Full rotational cycle of a constrained motor **C2n** in which an alkyl tether functions as a molecular spring. In the *Z*s isomer, the tether is not strained by the motor. When illuminated with UV light, the motor is converted into the *E*m isomer in which the tether is subjected to chemical strain which is further increased by a subsequent THI that forms **C2n**-*Es*. If the tether is long enough to skip over the motor core, the system can undergo another light-induced *E*/*Z* isomerization to form the *Z*m isomer, leading to a relaxation of chemical strain in the tether. Further relaxation by a THI yields the initial motor **C2n**-*Z*s. C) Macrocyclization of dihydroxy motor **OH** under high-dilution conditions by Williamson ether synthesis. D) X-ray structures of **OMe**-*Z*s, **OMe**-*Es*, **C8**-*Z*s, **C12**-*Z*s and **C12**-*Em*. Solvent molecules, hydrogen and disordered atoms are omitted for clarity. Ellipsoids are drawn at 50% probability.

by connecting their contra-rotating halves with molecular tethers, were reported by the Dube,[34,36] Giuseppone[59] and our group.[31] While the two latter AMMs[31,59] are bridged bismacrocyclic molecules that can induce twists in the tethers, the system by Dube and co-workers consists of a hemithioindigo motor and a biaryl unit both embedded within one macrocycle.[34,36] The light-driven, unidirectional motion of the hemithioindigo actuator induces a directed, coupled rotation of the biaryl moiety which can act as a hurdle that has to be overcome by the motor if the activation barrier for atropisomerization is sufficiently high. To get an even more systematic insight into the behavior of

a molecular motor that is subjected to varying amounts of mechanical stress, we wanted to investigate a paradigmatic system which allows for facile and stepwise adjustment of ring strain.

We accomplished our goal by linking the two contra-rotating parts of a first-generation Feringa motor with an alkyl tether, thereby forming macrocyclic structure **C2n** (with $n=4$–11). By systematically increasing the length of the alkyl chain—and thus the size of the macrocycles **C8**–**C22**—the degree of mechanical constraint on the movement of the motor can be precisely tuned and studied. Related strategies were successfully applied for hydrazone[56] and stilbene[53–55,57] photoswitches to investigate the influence of strain on their switchability or the reactivity of remote chemical bonds. It is important to note that switches usually undergo only one isomerization process, have no thermal ratcheting step and are therefore not unidirectional.[60,61] In stark contrast, a full motor rotation comprises four distinct isomerization steps, each of which can be potentially influenced by mechanical strain.

Results and Discussion

In our system, the alkyl tether functions as a molecular spring that is fully relaxed when motor **C2n** is in its *Z*s form (Figure 1B). Upon UV light illumination, the macrocyclized rotary motor undergoes an *E*/*Z* isomerization, leading to the formation of the *E*m isomer and to the build-up of chemical strain in the system, which is even further increased in the subsequent THI step that yields the *E*s isomer. Assuming that the alkyl tether is long enough to skip over one half of the motor core (Figure 1B), illumination with UV light induces an *E*/*Z* double bond isomerization which yields the *Z*m isomer that can undergo another THI to restore the initial *Z*s motor. We hypothesized that only tethers with sufficient length would enable a full motor rotation,[58] while tethers that are too short only allow for the first photochemical *E*/*Z* isomerization, thus preventing full rotation of the motor. We further anticipated that mechanical constraint should have a measurable effect on the THI steps.[34,36]

Constrained motors **C8**–**C22**-*Z*s were synthesized by macrocyclizing the *Z*s isomer of dihydroxy molecular motor **OH** with hydrocarbon chains in a Williamson ether synthesis under high-dilution conditions (Figure 1C).[62,63] The length of the alkyl chains ranges from octyl to docosyl (C_8H_{16} to $C_{22}H_{44}$) and was gradually increased by two methylene unit increments. We chose an even number of methylene units to avoid any influence of odd-even effects.[64] Molecular motors **C8**–**C22** were characterized by NMR spectroscopy, high-resolution mass spectrometry and in part by X-ray crystallography (Figure 1D).[65]

Indeed, we experimentally observed that mechanical strain has a significant effect on the switchability of the motor unit, as macrocycles **C8**–**C14** only undergo a photochemical *E*/*Z* isomerization and show no subsequent THI (Table 1 and Supporting Figures S1–S4, S10–S13 and S24–S27 and Tables S1–S3). ^{1}H NMR spectroscopy revealed that the photostationary state (PSS) is dependent on the macrocycle size (Figures 2A,B and Supporting Figures S1–S4). Motor **C8**-*Z*s forms the *E*m isomer in 50±2%, while the

Table 1: PSSs and energy differences (ΔG) between stable and metastable states and activation parameters (Gibbs free energy of activation ($\Delta G^{\ddagger}$), enthalpy of activation ($\Delta H^{\ddagger}$) and entropy of activation ($\Delta S^{\ddagger}$)) for THI and double bond isomerizations of macrocycles **C8**–**22** and reference compound **OMe**. PSSs were determined by ^{1}H NMR spectroscopy in toluene-d_8 at −20 °C and are given as the amount of product formed in the indicated (photo)reactions. Energies were determined by ^{1}H NMR spectroscopy in toluene-d_8 (1 mM) and are reported for 20 °C in kcal mol^{-1}. Activation parameters were determined by UV/Vis spectroscopy in octane (20 μM) and are reported for 20 °C. $\Delta H^{\ddagger}$ and $\Delta G^{\ddagger}$ are given in kcal mol^{-1}; $\Delta S^{\ddagger}$ is given in cal K^{-1} mol^{-1}.

	PSS		ΔG			$\Delta G^{\ddagger}$ ($\Delta H^{\ddagger}$, $\Delta S^{\ddagger}$)		
	(*Z*s→*E*m)	(*E*s→*Z*m)	(*E*m→*Z*s)	(*E*m→*E*s)	(*Z*m→*Z*s)	(*E*m→*Z*s)	(*E*m→*E*s)	(*Z*m→*Z*s)
C8	50±2%[a]	–	≤ −2.0	–	–	18.8±0.2 (18.2, −2.16)	–	–
C10	74±2%	–	≤ −2.0	–	–	25.3±0.1 (26.3, 3.56)	–	–
C12	81±2%	–	≤ −2.0	–	–	29.0±0.1[c] (29.8, 2.22)	–	–
C14	81±2%	–	≤ −2.0	–	–	≥32[c,d]	–	–
C16	83±2%	67±4%	–	+0.9±0.1	≤ −2.0	–	22.1±0.1 (14.1, −27.5)	23.6±0.2[e] (19.9, −12.5)
C18	80±2%	65±4%	–	−0.5±0.1	≤ −2.0	–	20.4±0.1 (18.1, −7.70)	23.7±0.1 (19.9, −12.8)
C20	81±2%	63±4%	–	−1.0±0.1	≤ −2.0	–	20.3±0.1 (17.3, −9.95)	23.7±0.1 (19.3, −15.0)
C22	80±2%	65±4%	–	−1.4±0.1	≤ −2.0	–	20.1±0.1 (18.6, −4.99)	23.7±0.1 (19.5, −14.4)
OMe	78±2%[b]	70±4%	–	≤ −2.0	≤ −2.0	–	18.6±0.3 (15.7, −9.99)	23.4±0.2 (19.5, −13.3)

[a] PSS determined at −40 °C. [b] PSS determined at −46 °C. [c] Energy given at 110 °C. [d] Energy estimated from a single relaxation at 110 °C. [e] Activation parameters determined by NMR spectroscopy in toluene-d_8.

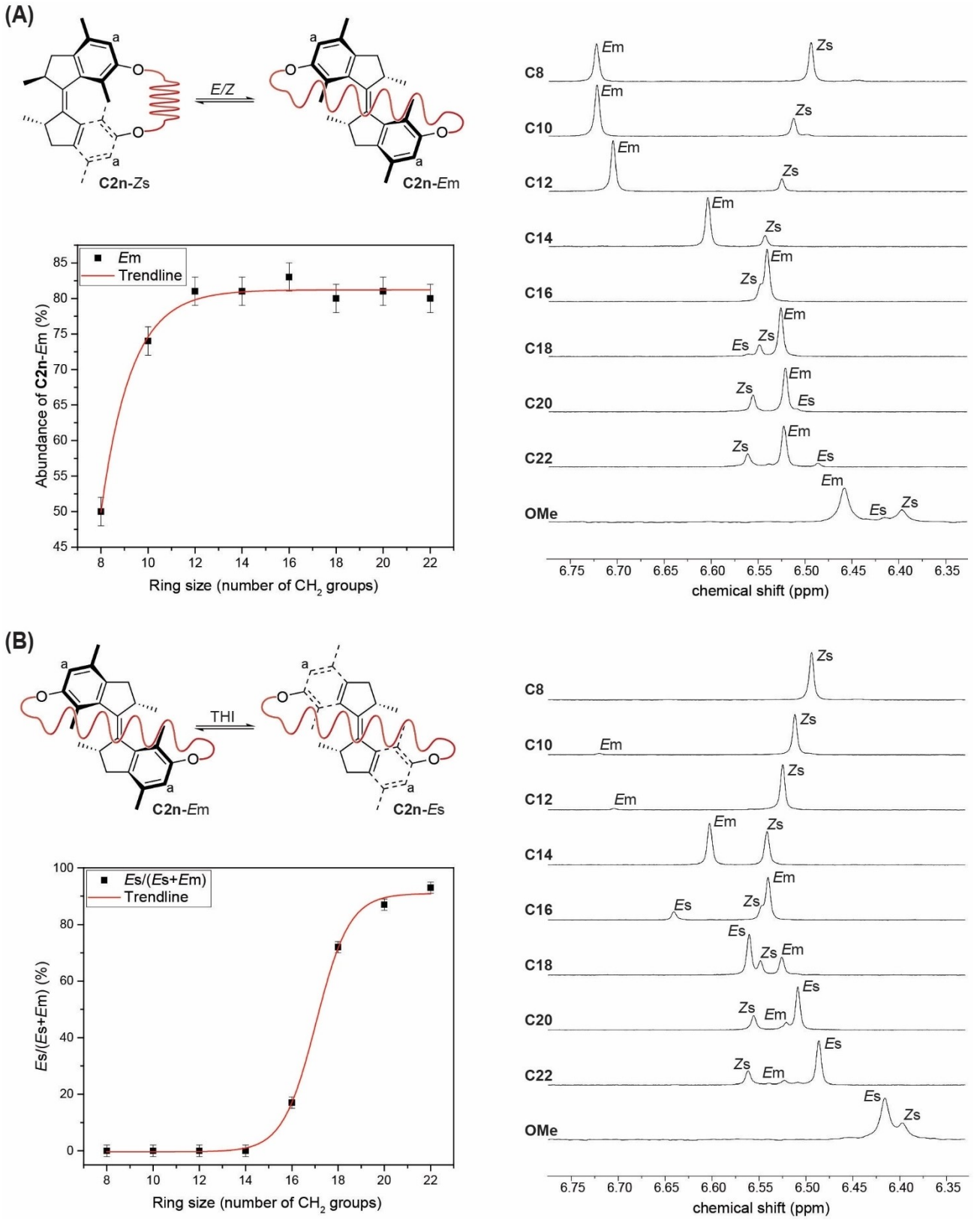

Figure 2. Photochemical *E*/*Z* isomerization and THI. A) The amount of *Em* isomer at PSS after UV light illumination increases with increasing ring size. The partial ^{1}H NMR spectra (toluene-d_8, 1 mM, −20 °C, 500 MHz) show the composition at PSS after illuminating pure **C8**–**22**-*Zs* and **OMe**-*Zs* samples with UV light. Only signals of the aromatic protons in position a are shown. B) The ratio of *Es* to *Em* isomer at PSS after UV light illumination increases with increasing ring size. The partial ^{1}H NMR spectra (toluene-d_8, 1 mM, −20 °C, 500 MHz) show the composition of pure **C8**–**22**-*Zs* and **OMe**-*Zs* samples that were illuminated with UV light to PSS and subsequently allowed to reach thermal equilibrium. Motor **C14** was partially equilibrated at 100 °C for 3 d. Only signals of the aromatic protons in position a are shown.

larger macrocycles **C10** and **C12**–**C14** reach up to 74±2% and 81±2%, respectively (Figure 2A, Table 1 and Supporting Table S1). Similarly, the activation barrier for the thermal *E*/*Z* back isomerization increases with increasing ring size (Table 1 and Supporting Table S3 and Figures S10–S13). Macrocycle **C8**-*E*m rapidly isomerizes back to **C8**-*Z*s with an activation barrier of $\Delta G_{C8}^{\ddagger}$ (*E*m→*Z*s)=18.8± 0.2 kcal mol^{-1}. For motors **C10**-*E*m and **C12**-*E*m the activation barrier increases dramatically with $\Delta G_{C10}^{\ddagger}$ (*E*m→*Z*s)= 25.3±0.1 kcal mol^{-1} and $\Delta G_{C12}^{\ddagger}$ (*E*m→*Z*s)=29.0± 0.1 kcal mol^{-1}, respectively. The thermal *E*/*Z* isomerization of isomer **C14**-*E*m is so slow that the activation energy for the process could only be estimated to be $\Delta G_{C14}^{\ddagger}$ (*E*m→ *Z*s) ≥ 32 kcal mol^{-1}. Interestingly, formation of the *E*s isomer was not observed by UV/Vis and NMR spectroscopy for motors **C8**–**C14**-*E*m, indicating that ring strain induced by the alkyl tethers inhibits the THI (Figure 2B).

To further investigate this behavior we performed single-crystal X-ray analyses of motors **OMe**-*E*s, **C12**-*Z*s and **C12**-*E*m (Figures 1D and 3A, B). The crystal structures suggest that skipping of the alkyl tether over the motor core is sterically unlikely (see space-filling models of **C12**-*Z*s and **C12**-*E*m in Figures 3A, B) and would form a highly strained species (for computational results see Figure 4). We also assume for **C8** and **C10** that the alkyl tether is unlikely to skip over the motor core as both macrocycles are smaller than **C12**. More importantly, a comparison with the reference compound **OMe**-*E*s indicates that the THI would induce additional ring strain in the system, since an inversion of the xylenyl moieties stretches the oligomeric tether even further (Figure 3B). In the case of the (*S*,*S*) **C12**-*E*m macrocycle, the alkyl tether as well as the oxygen atoms that connect it with the motor core face the *Si* side of the motor (with respect to the overcrowded double bond). Upon THI to form the *E*s isomer, the xylenyl units invert, pushing the

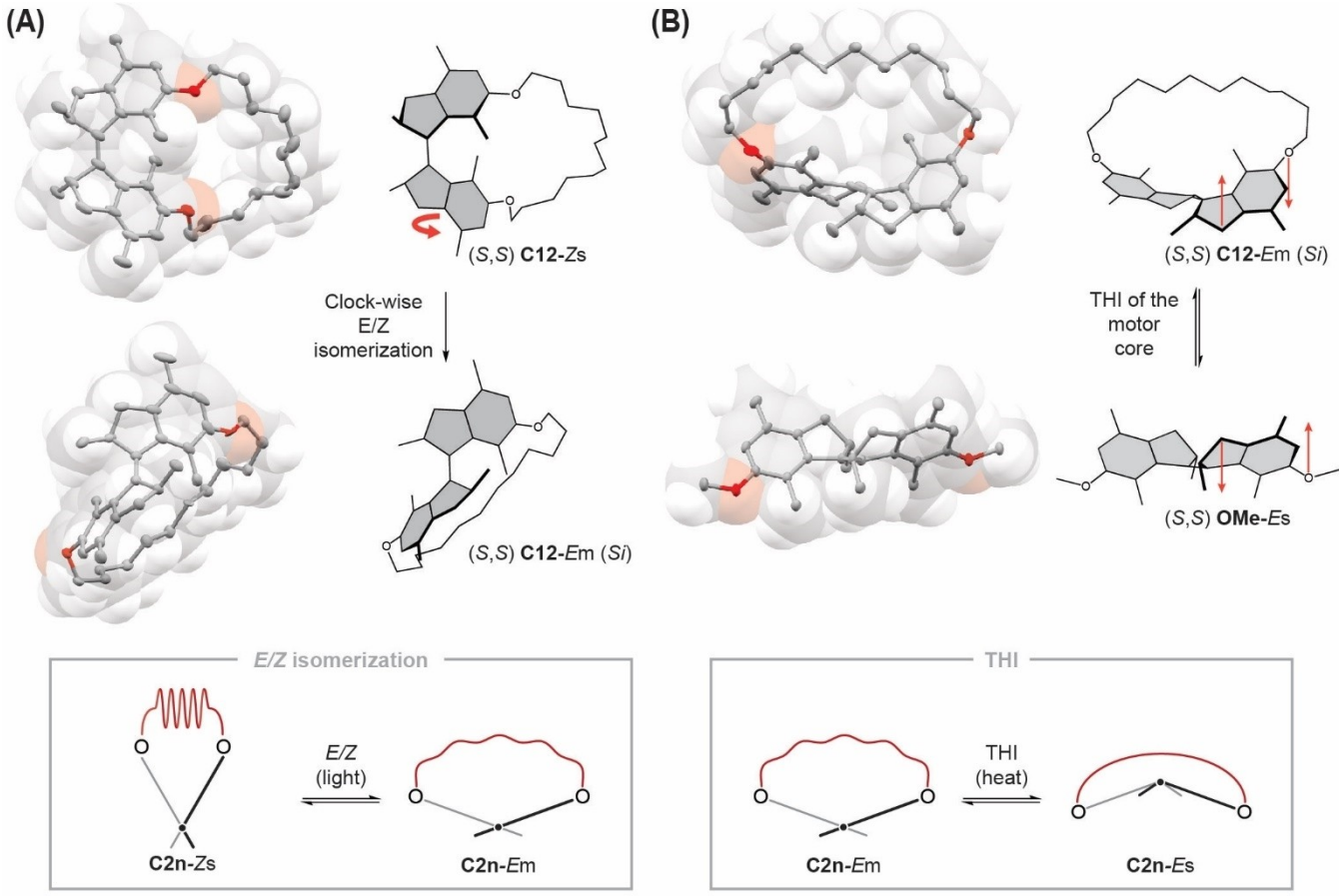

Figure 3. Unidirectional motor rotation and inhibition of helix inversion. A) The crystal structures of (*S*,*S*) **C12**-*Z*s and (*S*,*S*) **C12**-*E*m show that only a clockwise rotation of the bottom half of the motor (indicated by the red arrow) can position the dodecyl tether on the *Si* side of the molecule. The box shows the schematic structures of motor macrocycles **C2n**-*Z*s and **C2n**-*E*m with a view along the central double bond and the influence of an *E*/*Z* isomerization on the ring strain in the system. B) The crystal structure of (*S*,*S*) **C12**-*E*m shows that the alkyl tether is facing the *Si* side of the motor with respect to the central double bond. The oxygen atoms point in the same direction, thus minimizing strain in the system. The crystal structure of (*S*,*S*) **OMe**-*E*s indicates that a THI requires the oxygen atoms to move to the *Re* side of the motor. Therefore, a THI from (*S*,*S*) **C12**-*E*m (*Si*) to (*S*,*S*) **C12**-*E*s (*Re*) would increase the ring strain in the molecule. Red arrows indicate the direction of movement of the motor core to interconvert *E*m to *E*s and *vice versa*. The box shows the schematic structures of motor macrocycles **C2n**-*E*m and **C2n**-*E*s with a view along the central double bond and the influence of a THI on the ring strain in the system. All X-ray structures are depicted with a space-filling overlay. Hydrogen and disordered atoms are omitted for clarity. Ellipsoids are drawn at 50% probability.

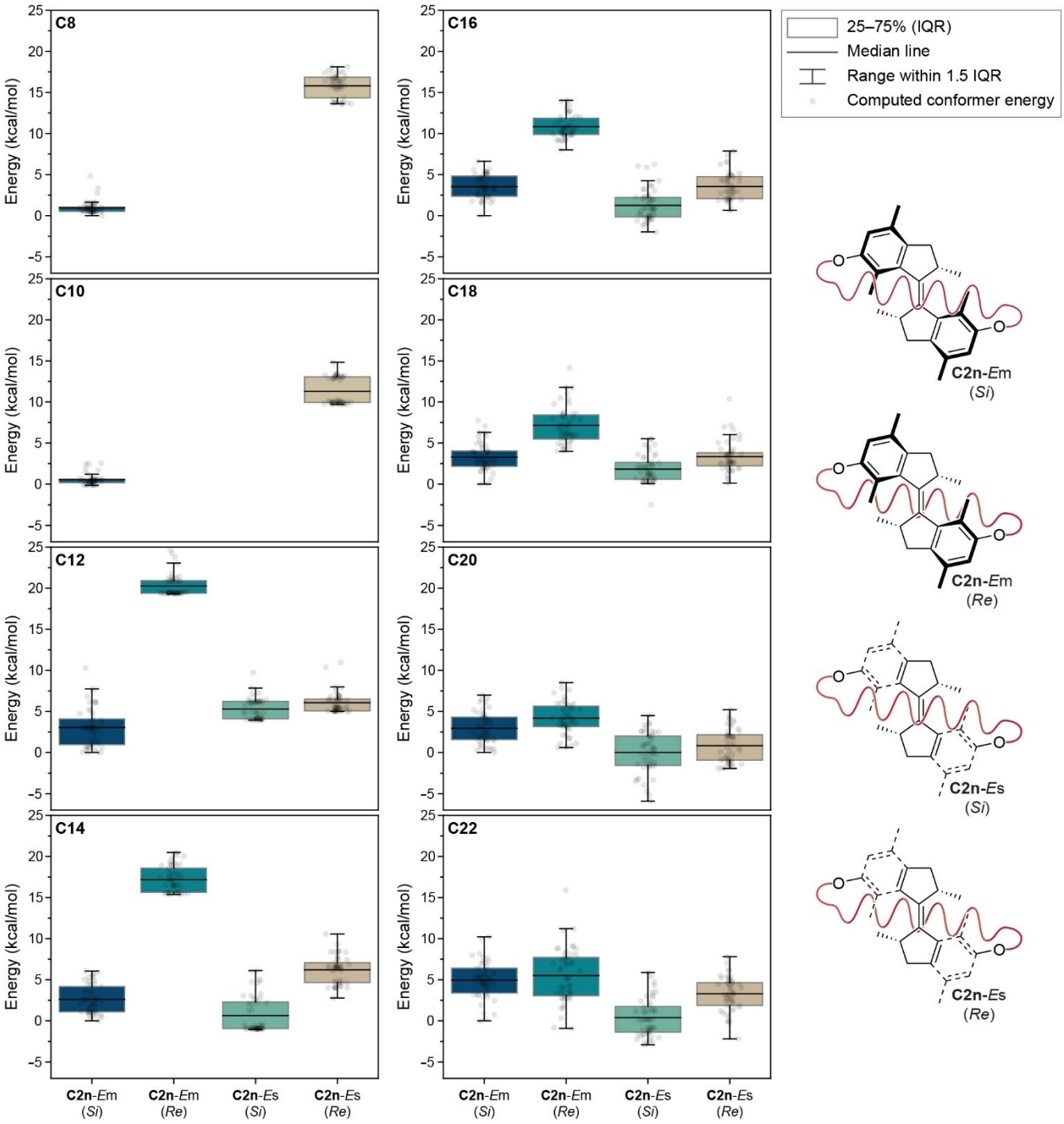

Figure 4. Box plots for the computed relative Gibbs free energies of **C2n**-*E*m (*Si*), **C2n**-*E*m (*Re*), **C2n**-*E*s (*Si*) and **C2n**-*E*s (*Re*). The computations lead to two main conclusions: i) in case of **C12**–**C16**-*E*m the energetically least favorable species are the ones with the alkyl tether on the *Re* side of the motor and ii) the relative energy difference between having the alkyl tether on the *Re* or *Si* side of the motor decreases with increasing ring size. Gibbs free energies were calculated at the r2SCAN-3c level of theory. The accuracy of the computational method is ≥ 1 kcal mol^{-1}, see reference [70].

oxygen atoms to the *Re* side of the motor. This movement would lead to an increase in ring strain in the system and is a likely reason why the THI from *E*m to *E*s in macrocycles **C8**–**C12** (and also **C14**, see Figure 4) does not occur. We also would like to emphasize that only thanks to the relative mechanochemical stabilization of the **C12**-*E*m isomer, we could obtain the first unambiguous structural characterization of the usually thermally labile *E*m isomer by X-ray analysis. Additionally, the alkyl tether allows for tracking of the motor movement (Figure 3A). The alkyl chain follows

the rotation of the motor and is located on the *Si* side of the (*S,S*) **C12**-*E*m motor (*Re* side for (*R,R*) **C12**-*E*m) after the photoreaction. Therefore, the only plausible direction of rotation of **C12**-*Z*s to form **C12**-*E*m is clockwise for the (*S,S*) and counterclockwise for the (*R,R*) diastereomer. This gives unprecedented structural insight into the mechanism of molecular rotary motors based on the Feringa design.

By further increasing the ring size of the macrocycles, full rotation in motors **C16–C22** was observed (Table 1 and Supporting Figures S5–S9, S14–S23 and S28–S32 and Tables S1–S3). According to ^{1}H NMR spectroscopy, the length of the tether from **C16** onward has no measurable effect on the photochemical steps in the rotational cycle (Supporting Figures S5–S9). The PSS ratio for the photoreaction of **C16–C22**-*E*s and **OMe**-*E*s to the respective *Z*m isomer is similar and leads to the formation of *Z*m in $\approx 66 \pm 4\,\%$ (Figure 2A). Also, the PSS ratio for the photochemical double bond isomerization from the *Z*s to the respective *E*m diastereomer is not affected by larger macrocycles and is the same for motors **C12–C22** and **OMe** forming the *E*m isomer in $\approx 80 \pm 2\,\%$ (Figure 2A). Looking at the thermal steps, we did not observe a significant dependence of the THI from **C16–C22**-*Z*m and **OMe**-*Z*m to the respective *Z*s isomer on the length (or presence) of the alkyl tethers. All reactions are exergonic and irreversible with ΔG (*Z*m→*Z*s) $\leq -2.0\,\mathrm{kcal\,mol^{-1}}$ and $\Delta G^{\ddagger}$ (*Z*m→*Z*s) $\approx 23.7 \pm 0.1\,\mathrm{kcal\,mol^{-1}}$. However, the THI from **C16–C22**-*E*m to the respective *E*s isomer does depend on the size of the macrocycle (Figure 2B). The THI repositions the allylic methyl groups from an energetically less favored *pseudo*-equatorial into a more favorable *pseudo*-axial position (Figures 1A, B and 3B). While this process releases tension in the motor unit, ring strain hampers the THI and destabilizes the *E*s relative to the *E*m isomers (Table 1). By increasing the length of the alkyl tether from hexadecyl to docosyl the formation of *E*s becomes increasingly favored energetically, ranging from $\Delta G_{\mathbf{C16}}$ (*E*m→*E*s) $= 0.9 \pm 0.1\,\mathrm{kcal\,mol^{-1}}$ to $\Delta G_{\mathbf{C22}}$ (*E*m→*E*s) $= -1.4 \pm 0.1\,\mathrm{kcal\,mol^{-1}}$ with activation energies of $\Delta G_{\mathbf{C16}}{}^{\ddagger}$ (*E*m→*E*s) $= 22.1 \pm 0.1\,\mathrm{kcal\,mol^{-1}}$ and $\Delta G_{\mathbf{C22}}{}^{\ddagger}$ (*E*m→*E*s) $= 20.1 \pm 0.1\,\mathrm{kcal\,mol^{-1}}$ (a similar dependence of THI activation barriers in hemithioindigo motors on ring strain was also observed by Dube and co-workers).[34,36] Consequently, the THI from **C16**-*E*m to **C16**-*E*s is endergonic (please note: **C16**-*E*m is thermodynamically more stable than **C16**-*E*s), with a (comparably) low activation entropy of $\Delta S_{\mathbf{C16}}{}^{\ddagger}$ (*E*m→*E*s) $= -27.5\,\mathrm{cal\,K^{-1}\,mol^{-1}}$ suggesting that the transition state is particularly structured and conformationally restricted. Nonetheless, the rotation for **C16** is still unidirectional, since the THI from **C16**-*Z*m to **C16**-*Z*s is irreversible ($\Delta G_{\mathbf{C16}}$ (*Z*m→*Z*s) $\leq -2.0\,\mathrm{kcal\,mol^{-1}}$) and thus energetically more favorable than the THI from **C16**-*E*m to **C16**-*E*s. By comparing these energy differences with the uncyclized model compound **OMe** ($\Delta G_{\mathbf{OMe}}$ (*E*m→*E*s) $\leq -2.0\,\mathrm{kcal\,mol^{-1}}$ and $\Delta G_{\mathbf{OMe}}{}^{\ddagger}$ (*E*m→*E*s) $= 18.6 \pm 0.3\,\mathrm{kcal\,mol^{-1}}$) we can show that ring strain makes the formation of the *E*s isomer kinetically and thermodynamically less favorable.

The fact that molecular motors **C16–C22** perform a full rotational cycle implies that a skipping of the tether over the motor core is kinetically feasible.[58] The mechanism of such a skipping event could be mechanistically elucidated for hemithioindigo motors by using a biaryl unit as an "energy hurdle".[36] However, we were not able to directly measure such a "skipping rope" process experimentally (only one distinct species per motor diastereomer was observed). Therefore, we performed a computational study to elucidate the relative thermodynamic stability of motors **C2n**-*E*m and **C2n**-*E*s with the alkyl tether on the *Re* or *Si* side of the motor core, which provides further information about the distribution of such species in equilibrium.

Motor structures **C2n**-*E*m (*Si*), **C2n**-*E*m (*Re*), **C2n**-*E*s (*Si*) and **C2n**-*E*s (*Re*) were pre-screened via a preliminary metadynamics run of 2 ns (2 fs step, 298.15 K using a Berendsen thermostat) using the GFN force field implemented in xTB 6.4.1.[66] Subsequently, 50 geometries were randomly extracted and re-optimized with the composite functional r^{2}SCAN-3c,[67] as implemented in the Orca 5.0.1 package,[68] and the thermochemical data were calculated at the same level of theory. Finally, the relative Gibbs free energies (with respect to the most stable **C2n**-*E*m (*Si*) geometry) were computed taking into account the electronic energies calculated at the r^{2}SCAN-3c, pW6B95/def2-TZVP,gCP(TZ) or ωB97X-V/def2-TZVP,gCP(TZ) levels of theory (Figure 4 and Supporting Data File).[69,70] The calculations indicate that positioning the alkyl chain on the *Re* side of motors **C12–C16**-*E*m is thermodynamically unlikely, as the *E*m (*Re*) species has the highest median energy in these cases (note that the structures of **C8**- and **C10**-*E*s (*Re*) and -*E*m (*Si*) could not be modeled, as they were not found to be minima on the potential energy surface of these motors). Furthermore, our computational analysis shows the general trend that increasing the ring size of motors **C2n**-*E*m and **C2n**-*E*s decreases the relative energy differences between species in which the alkyl chain faces the *Re* or *Si* side of the molecule. In case of **C18–C22**-*E*m and **C18–C22**-*E*s, the energies of the computed structures are comparable indicating that the alkyl tether can be localized on the *Re* and *Si* side of the motor.

Conclusion

Our systematic study shows that chemical strain has a significant impact on the thermal *and* photochemical steps in a 360° rotational cycle of a first-generation molecular motor. We observed that the PSS from *Z*s to *E*m, the thermal double bond isomerization from *E*m to *Z*s and THI from *E*m to *E*s in motor macrocycles **C2n** are dependent on ring strain. The alkyl tethers in macrocycles **C8–C14** are so short that the motor unit can only undergo a photochemical *E*/*Z* isomerization from *Z*s to *E*m, while subsequent THI was not observed. Instead, motors **C16–C22** can perform a 360° rotation, but ring strain hampers the formation of the *E*s isomer by THI. Furthermore, we could use the relative stabilization of the *E*m isomer of motor **C12** to gain unprecedented structural insight into the operational routine of a rotary molecular motor by single-crystal X-ray analysis. We anticipate that our findings will serve as a blueprint and

open up design space for the development of more complex molecular machinery.

Acknowledgements

We gratefully acknowledge the generous support from the Alexander von Humboldt Foundation (Feodor Lynen Research Fellowship to M.K.), the Marie Skłodowska-Curie Actions (Individual Fellowship 838280 to S.C.), the Horizon 2020 Framework Program (ERC Advanced Investigator Grant No. 694345 to B.L.F.) and the Ministry of Education, Culture and Science of the Netherlands (Gravitation Program No. 024.001.035 to B.L.F.). We would like to thank the Center for Information Technology of the University of Groningen for their support and for providing access to the Peregrine high performance computing cluster.

Conflict of Interest

The authors declare no conflict of interest.

Data Availability Statement

The data that support the findings of this study are available in the Supporting Information of this article.

Keywords: Macrocycles · Molecular Motors · Photochemistry · Strained Molecules

[1] M. Schliwa, *Molecular Motors*, Wiley-VCH, Weinheim, **2006**.
[2] D. S. Goodsell, *The Machinery of Life*, Springer, New York, **2009**.
[3] V. Balzani, A. Credi, F. M. Raymo, J. F. Stoddart, *Angew. Chem. Int. Ed.* **2000**, *39*, 3348–3391; *Angew. Chem.* **2000**, *112*, 3484–3530.
[4] J.-P. Sauvage, *Molecular Machines and Motors*, Springer, Berlin, **2001**.
[5] W. R. Browne, B. L. Feringa, *Nat. Nanotechnol.* **2006**, *1*, 25–35.
[6] E. R. Kay, D. A. Leigh, F. Zerbetto, *Angew. Chem. Int. Ed.* **2007**, *46*, 72–191; *Angew. Chem.* **2007**, *119*, 72–196.
[7] V. Balzani, A. Credi, M. Venturi, *Molecular Devices and Machines: Concepts and Perspectives for the Nanoworld*, Wiley-VCH, Weinheim, **2008**.
[8] I. Aprahamian, *ACS Cent. Sci.* **2020**, *6*, 347–358.
[9] Y. Feng, M. Ovalle, J. S. W. Seale, C. K. Lee, D. J. Kim, R. D. Astumian, J. F. Stoddart, *J. Am. Chem. Soc.* **2021**, *143*, 5569–5591.
[10] A. Coskun, M. Banaszak, R. D. Astumian, J. F. Stoddart, B. A. Grzybowski, *Chem. Soc. Rev.* **2012**, *41*, 19–30.
[11] R. D. Astumian, *Chem. Sci.* **2017**, *8*, 840–845.
[12] J. Wang, B. L. Feringa, *Science* **2011**, *331*, 1429–1432.
[13] M. Vlatković, L. Bernardi, E. Otten, B. L. Feringa, *Chem. Commun.* **2014**, *50*, 7773–7775.
[14] S. F. Pizzolato, P. Štacko, J. C. M. Kistemaker, T. van Leeuwen, B. L. Feringa, *Nat. Catal.* **2020**, *3*, 488–496.
[15] R. Eelkema, M. M. Pollard, J. Vicario, N. Katsonis, B. S. Ramon, C. W. M. Bastiaansen, D. J. Broer, B. L. Feringa, *Nature* **2006**, *440*, 163.
[16] S. Iamsaard, S. J. Aßhoff, B. Matt, T. Kudernac, J. J. L. M. Cornelissen, S. P. Fletcher, N. Katsonis, *Nat. Chem.* **2014**, *6*, 229–235.
[17] Q. Li, G. Fuks, E. Moulin, M. Maaloum, M. Rawiso, I. Kulic, J. T. Foy, N. Giuseppone, *Nat. Nanotechnol.* **2015**, *10*, 161–165.
[18] J. T. Foy, Q. Li, A. Goujon, J.-R. Colard-Itté, G. Fuks, E. Moulin, O. Schiffmann, D. Dattler, D. P. Funeriu, N. Giuseppone, *Nat. Nanotechnol.* **2017**, *12*, 540–545.
[19] J. Chen, F. K. C. Leung, M. C. A. Stuart, T. Kajitani, T. Fukushima, E. Van Der Giessen, B. L. Feringa, *Nat. Chem.* **2018**, *10*, 132–138.
[20] J.-R. Colard-Itté, Q. Li, D. Collin, G. Mariani, G. Fuks, E. Moulin, E. Buhler, N. Giuseppone, *Nanoscale* **2019**, *11*, 5197–5202.
[21] A. Ryabchun, Q. Li, F. Lancia, I. Aprahamian, N. Katsonis, *J. Am. Chem. Soc.* **2019**, *141*, 1196–1200.
[22] J. Hou, A. Mondal, G. Long, L. de Haan, W. Zhao, G. Zhou, D. Liu, D. J. Broer, J. Chen, B. L. Feringa, *Angew. Chem. Int. Ed.* **2021**, *60*, 8251–8257; *Angew. Chem.* **2021**, *133*, 8332–8338.
[23] A. Koçer, M. Walko, W. Meijberg, B. L. Feringa, *Science* **2005**, *309*, 755–758.
[24] V. García-López, F. Chen, L. G. Nilewski, G. Duret, A. Aliyan, A. B. Kolomeisky, J. T. Robinson, G. Wang, R. Pal, J. M. Tour, *Nature* **2017**, *548*, 567–572.
[25] N. L. Mutter, J. Volarić, W. Szymanski, B. L. Feringa, G. Maglia, *J. Am. Chem. Soc.* **2019**, *141*, 14356–14363.
[26] B. Lewandowski, G. De Bo, J. W. Ward, M. Papmeyer, S. Kuschel, M. J. Aldegunde, P. M. E. Gramlich, D. Heckmann, S. M. Goldup, D. M. D'Souza, A. E. Fernandes, D. A. Leigh, *Science* **2013**, *339*, 189–193.
[27] J. Chen, S. J. Wezenberg, B. L. Feringa, *Chem. Commun.* **2016**, *52*, 6765–6768.
[28] S. Kassem, A. T. L. Lee, D. A. Leigh, A. Markevicius, J. Solà, *Nat. Chem.* **2016**, *8*, 138–143.
[29] S. Kassem, A. T. L. Lee, D. A. Leigh, V. Marcos, L. I. Palmer, S. Pisano, *Nature* **2017**, *549*, 374–378.
[30] H. Sell, A. Gehl, D. Plaul, F. D. Sönnichsen, C. Schütt, F. Köhler, K. Steinborn, R. Herges, *Commun. Chem.* **2019**, *2*, 62.
[31] M. Kathan, S. Crespi, N. O. Thiel, D. L. Stares, D. Morsa, J. de Boer, G. Pacella, T. van den Enk, P. Kobauri, G. Portale, C. A. Schalley, B. L. Feringa, *Nat. Nanotechnol.* **2022**, *17*, 159–165.
[32] T. Muraoka, K. Kinbara, T. Aida, *Nature* **2006**, *440*, 512–515.
[33] P. Štacko, J. C. M. Kistemaker, T. van Leeuwen, M.-C. Chang, E. Otten, B. L. Feringa, *Science* **2017**, *356*, 964–968.
[34] E. Uhl, S. Thumser, P. Mayer, H. Dube, *Angew. Chem. Int. Ed.* **2018**, *57*, 11064–11068; *Angew. Chem.* **2018**, *130*, 11231–11235.
[35] J. J. Yu, L. Y. Zhao, Z. T. Shi, Q. Zhang, G. London, W. J. Liang, C. Gao, M. M. Li, X. M. Cao, H. Tian, B. L. Feringa, D.-H. Qu, *J. Org. Chem.* **2019**, *84*, 5790–5802.
[36] E. Uhl, P. Mayer, H. Dube, *Angew. Chem. Int. Ed.* **2020**, *59*, 5730–5737; *Angew. Chem.* **2020**, *132*, 5779–5786.
[37] N. N. Bach, V. Josef, H. Maid, H. Dube, *Angew. Chem. Int. Ed.* **2022**, *61*, e202201882; *Angew. Chem.* **2022**, *134*, e202201882.
[38] G. Ragazzon, M. Baroncini, S. Silvi, M. Venturi, A. Credi, *Nat. Nanotechnol.* **2015**, *10*, 70–75.
[39] C. Cheng, P. R. McGonigal, S. T. Schneebeli, H. Li, N. A. Vermeulen, C. Ke, J. F. Stoddart, *Nat. Nanotechnol.* **2015**, *10*, 547–553.
[40] Y. Qiu, L. Zhang, C. Pezzato, Y. Feng, W. Li, M. T. Nguyen, C. Cheng, D. Shen, Q. H. Guo, Y. Shi, K. Cai, F. M. Alsubaie, R. D. Astumian, J. F. Stoddart, *J. Am. Chem. Soc.* **2019**, *141*, 17472–17476.
[41] Y. Qiu, B. Song, C. Pezzato, D. Shen, W. Liu, L. Zhang, Y. Feng, Q. Guo, K. Cai, W. Li, H. Chen, M. T. Nguyen, Y. Shi,

C. Cheng, R. D. Astumian, X. Li, J. F. Stoddart, *Science* **2020**, *368*, 1247–1253.
[42] L. Feng, Y. Qiu, Q.-H. Guo, Z. Chen, J. S. W. Seale, K. He, H. Wu, Y. Feng, O. K. Farha, R. D. Astumian, J. F. Stoddart, *Science* **2021**, *374*, 1215–1221.
[43] S. Amano, S. D. P. Fielden, D. A. Leigh, *Nature* **2021**, *594*, 529–534.
[44] N. Koumura, R. W. J. Zijistra, R. A. Van Delden, N. Harada, B. L. Feringa, *Nature* **1999**, *401*, 152–155.
[45] N. Koumura, E. M. Geertsema, M. B. Van Gelder, A. Meetsma, B. L. Feringa, *J. Am. Chem. Soc.* **2002**, *124*, 5037–5051.
[46] L. Greb, J. M. Lehn, *J. Am. Chem. Soc.* **2014**, *136*, 13114–13117.
[47] J. C. M. Kistemaker, P. Štacko, J. Visser, B. L. Feringa, *Nat. Chem.* **2015**, *7*, 890–896.
[48] D. Roke, S. J. Wezenberg, B. L. Feringa, *Proc. Natl. Acad. Sci. USA* **2018**, *115*, 9423–9431.
[49] V. García-López, D. Liu, J. M. Tour, *Chem. Rev.* **2020**, *120*, 79–124.
[50] D. R. S. Pooler, A. S. Lubbe, S. Crespi, B. L. Feringa, *Chem. Sci.* **2021**, *12*, 14964–14986.
[51] R. Costil, M. Holzheimer, S. Crespi, N. A. Simeth, B. L. Feringa, *Chem. Rev.* **2021**, *121*, 13213–13237.
[52] T. Hugel, N. B. Holland, A. Cattani, L. Moroder, M. Seitz, H. E. Gaub, *Science* **2002**, *296*, 1103–1106.
[53] Z. Huang, Q.-Z. Yang, D. Khvostichenko, T. J. Kucharski, J. Chen, R. Boulatov, *J. Am. Chem. Soc.* **2009**, *131*, 1407–1409.
[54] Q.-Z. Yang, Z. Huang, T. J. Kucharski, D. Khvostichenko, J. Chen, R. Boulatov, *Nat. Nanotechnol.* **2009**, *4*, 302–306.
[55] S. Akbulatov, Y. Tian, Z. Huang, T. J. Kucharski, Q.-Z. Yang, R. Boulatov, *Science* **2017**, *357*, 299–303.
[56] Q. Li, H. Qian, B. Shao, R. P. Hughes, I. Aprahamian, *J. Am. Chem. Soc.* **2018**, *140*, 11829–11835.
[57] S. Olsson, Ó. B. Pérez, M. Blom, A. Gogoll, *Beilstein J. Org. Chem.* **2019**, *15*, 2408–2418.
[58] Y. Liu, Q. Zhang, S. Crespi, S. Chen, X.-K. Zhang, T.-Y. Xu, C.-S. Ma, S.-W. Zhou, Z.-T. Shi, H. Tian, B. L. Feringa, D.-H. Qu, *Angew. Chem. Int. Ed.* **2021**, *60*, 16129–16138; *Angew. Chem.* **2021**, *133*, 16265–16274.
[59] C. Gao, A. V. Jentzsch, E. Moulin, N. Giuseppone, *J. Am. Chem. Soc.* **2022**, *144*, 9845–9852.
[60] B. L. Feringa, W. R. Browne, *Molecular Switches*, Wiley-VCH, Weinheim, **2011**.
[61] M. Kathan, S. Hecht, *Chem. Soc. Rev.* **2017**, *46*, 5536–5550.
[62] B. K. Vriesema, J. Buter, R. M. Kellogg, *J. Org. Chem.* **1984**, *49*, 110–113.
[63] V. Martí-Centelles, M. D. Pandey, M. I. Burguete, S. V. Luis, *Chem. Rev.* **2015**, *115*, 8736–8834.
[64] J. A. Pradeilles, S. Zhong, M. Baglyas, G. Tarczay, C. P. Butts, E. L. Myers, V. K. Aggarwal, *Nat. Chem.* **2020**, *12*, 475–480.
[65] Deposition Numbers 2165821, 2165822, 2165823, 2165824, 2165825 contain the supplementary crystallographic data for this paper. These data are provided free of charge by the joint Cambridge Crystallographic Data Centre and Fachinformationszentrum Karlsruhe Access Structures service.
[66] C. Bannwarth, S. Ehlert, S. Grimme, *J. Chem. Theory Comput.* **2019**, *15*, 1652–1671.
[67] S. Grimme, A. Hansen, S. Ehlert, J. M. Mewes, *J. Chem. Phys.* **2021**, *154*, 064103.
[68] F. Neese, F. Wennmohs, U. Becker, C. Riplinger, *J. Chem. Phys.* **2020**, *152*, 224108.
[69] L. Goerigk, A. Hansen, C. Bauer, S. Ehrlich, A. Najibi, S. Grimme, *Phys. Chem. Chem. Phys.* **2017**, *19*, 32184–32215.
[70] M. Bursch, J.-M. Mewes, A. Hansen, S. Grimme, *ChemRxiv* **2022**, https://doi.org/10.26434/chemrxiv-2022-n304h. This content is a preprint and has not been peer-reviewed.

Manuscript received: April 20, 2022
Accepted manuscript online: June 19, 2022
Version of record online: July 13, 2022